A&A 531, L8 (2011)
DOI: 10.1051/0004-6361/201117170

Astronomy & Astrophysics

Letter to the Editor

Detection of interstellar hydrogen peroxide⋆

P. Bergman[1], B. Parise[2], R. Liseau[3], B. Larsson[4], H. Olofsson[1], K. M. Menten[2], and R. Güsten[2]

[1] Onsala Space Observatory, Chalmers University of Technology, 439 92 Onsala, Sweden
e-mail: per.bergman@chalmers.se
[2] Max Planck Institut für Radioastronomie, Auf dem Hügel 69, 53121 Bonn, Germany
[3] Department of Earth and Space Sciences, Chalmers University of Technology, 439 92 Onsala, Sweden
[4] Department of Astronomy, Stockholm University, AlbaNova, 10691 Stockholm, Sweden

Received 2 May 2011 / Accepted 25 May 2011

ABSTRACT

Context. The molecular species hydrogen peroxide, HOOH, is likely to be a key ingredient in the oxygen and water chemistry in the interstellar medium.
Aims. Our aim with this investigation is to determine how abundant HOOH is in the cloud core ρ Oph A.
Methods. By observing several transitions of HOOH in the (sub)millimeter regime we seek to identify the molecule and also to determine the excitation conditions through a multilevel excitation analysis.
Results. We have detected three spectral lines toward the SM1 position of ρ Oph A at velocity-corrected frequencies that coincide very closely with those measured from laboratory spectroscopy of HOOH. A fourth line was detected at the 4σ level. We also found through mapping observations that the HOOH emission extends (about 0.05 pc) over the densest part of the ρ Oph A cloud core. We derive an abundance of HOOH relative to that of H_2 in the SM1 core of about 1×10^{-10}.
Conclusions. To our knowledge, this is the first reported detection of HOOH in the interstellar medium.

Key words. astrochemistry – ISM: abundances – ISM: individual objects: ρ Oph A – ISM: molecules

1. Introduction

Hydrogen peroxide, HOOH, is believed to play an important role in the Earth's atmospheric ozone and water chemistry. It is a key constituent in the gas- and liquid-phase radical chemistry and has an oxidizing potential in the liquid phase. Gas-phase HOOH has been seen in the Martian atmosphere by ground-based observations (Clancy et al. 2004; Encrenaz et al. 2004). However, recent Mars observations with the *Herschel* Observatory (Hartogh et al. 2010) failed to detect HOOH at levels below those previously seen. The non-detection was attributed to seasonal variations.

Interestingly, HOOH is among the simplest molecules that show internal rotation. The internal rotation, or torsion, manifests itself as a rotation of the two O–H bonds about the O–O bond. This hindered internal rotation can be described with a torsion potential in which the two minima (the most stable configurations) do not coincide with the *cis* or *trans* alignment of the two O–H bonds[1]. The twofold barrier gives rise to a quartet of sublevels for each torsional state. These sublevels are denoted $\tau = 1, 2, 3, 4$ (Hunt et al. 1965). Moreover, HOOH is a light, slightly asymmetric prolate rotor (belonging to the $C_{2h}^{\dagger}$ point group, see Hougen 1984, for a discussion), with only *c*-type transitions and with a dipole moment of 1.6 D (Cohen & Pickett 1981; Perrin et al. 1996). Because of this, no pure rotational transitions occur, and only transitions corresponding to a combined ro-torsional motion change can take place. The mm and submm spectrum of HOOH has been studied rather extensively in the laboratory (Helminger et al. 1981; Petkie et al. 1995) and is available in the JPL database (Pickett et al. 1998).

To our knowledge, HOOH has not so far been detected in the interstellar medium. Also, very few abundance limits have been reported. Blake et al. (1987) derived an upper limit for HOOH of 4.5×10^{-10} with respect to H_2 from their Orion spectral scan data. Boudin et al. (1998) reported an upper limit of 5.2% of solid HOOH relative to H_2O ice toward NGC 7538 IRS9.

As in the Earth's atmosphere, HOOH is expected to be closely connected to the water and molecular oxygen chemistry also for those physical conditions prevailing in molecular clouds. In current pure gas-phase models, HOOH is formed by reaction of H_2 with HO_2 or via the reaction involving two OH radicals. However, these reactions proceed very slowly[2]. Alternatively, Tielens & Hagen (1982) suggested that HOOH could be formed on grain surfaces by the successive additions of H atoms to molecular oxygen. If this is the case, HOOH could be closely related to the amount of O_2 on grains.

The 119 GHz line of O_2 was detected toward the cloud ρ Oph A with an abundance of 5×10^{-8} relative to H_2 by Larsson et al. (2007) using the Odin satellite. The ρ Oph A molecular cloud, at a distance of about 120 pc, has been the subject of several studies. Continuum observations (André et al. 1993; Motte et al. 1998) and $C^{18}O$ observations (Liseau et al. 2010) revealed

⋆ Based on observations with the Atacama Pathfinder EXperiment (APEX) telescope. APEX is a collaboration between the Max-Planck-Institut für Radioastronomie, the European Southern Observatory, and the Onsala Space Observatory.

[1] When the two O–H bonds point in the same direction, this is referred to as the *cis* position, while the 180 degree opposite case is called the *trans* position. For HOOH, the *trans* potential barrier height is 557 K, while the *cis* barrier height is almost 4000 K (Pelz et al. 1993).

[2] http://www.physics.ohio-state.edu/~eric

Table 1. Observed HOOH lines.

Frequency (MHz)	Transition $J'_{K'_a,K'_c}-J''_{K''_a,K''_c}$	$\tau'-\tau''$	E_u (K)	A_{ul} (s^{-1})
219 166.86	$3_{0,3}-2_{1,1}$	4–2	31.2	8.58×10^{-5}
251 914.68	$6_{1,5}-5_{0,5}$	2–4	65.5	2.46×10^{-4}
268 961.17	$4_{0,4}-3_{1,2}$	4–2	41.1	1.84×10^{-4}
318 222.52	$5_{0,5}-4_{1,3}$	4–2	53.4	3.31×10^{-4}
318 712.10	$5_{1,4}-6_{0,6}$	3–1	67.0	4.12×10^{-4}
670 595.82	$1_{1,0}-0_{0,0}$	3–1	32.2	5.79×10^{-3}

several cores. Very recently, Bergman and coworkers found a very high degree of deuteration toward the SM1 core in ρ Oph A from observations of deuterated H_2CO (Bergman et al. 2011). These observations suggest that grain surface reactions were at work to produce the very high deuterium levels observed in the gas-phase material.

In this Letter we continue our study of the ρ Oph A cloud by reporting on observations of several HOOH transitions. We have detected four HOOH lines and two of these lines were mapped over the central part of this cloud. In Sect. 2 we describe our observations and present our results. There, we also describe in more detail the energy level structure and symmetry of HOOH, which is important for discussing the detected lines. Then, in Sect. 3, we discuss the implications of our results.

2. Observations and results

We have used the APEX 12 m telescope located at about 5100 m altitude in the Chilean Andes (Güsten et al. 2006) to observe HOOH. For the lower frequency lines we used the Swedish heterodyne facility instruments APEX-1 and APEX-2 (Vassilev et al. 2008). The 7-pixel longer wavelength (450 μm) module of the MPIfR-built CHAMP$^+$ receiver array (Kasemann et al. 2006) was used for the observations of a high-frequency line. The 7 pixels, spaced by 18″, are arranged in a hexagon around a central pixel. The observations took place on several occasions during 2010; April 2–11, July 7, August 4–8, and September 10–13.

The targeted HOOH lines are listed in Table 1. The frequency, transition quantum number designation, energy of upper level, and Einstein A-coefficient are listed. All values have been compiled from the JPL catalogue (Pickett et al. 1998). The frequency uncertainty for the listed lines is 0.1 MHz or better and this corresponds to 0.14 km s^{-1} at 219 GHz. We also present in Fig. 1 the energy diagrams for all levels below 100 K. Owing to the symmetry of HOOH, four different radiatively decoupled ladders occur: $A_{1\leftrightarrow3}$, $A_{2\leftrightarrow4}$, $B_{1\leftrightarrow3}$, and $B_{2\leftrightarrow4}$. The subscript indicates the pair of torsional quantum numbers τ involved. The c-type electric dipole transitions must also obey $\tau = 1 \leftrightarrow 3$ or $\tau = 2 \leftrightarrow 4$ (Hunt et al. 1965) and are drawn as downward arrows connecting the upper and lower levels in Fig. 1. The A-species have a nuclear spin weight of 1 and the B-species have a spin weight of 3 (Hougen 1984). This is, of course, due to the nuclear spin directions of the two H atoms (in the same way as the ortho and para symmetries occur for H_2O or H_2CO).

The ground-state symmetry species is that of $A_{1\leftrightarrow3}$ with the $B_{1\leftrightarrow3}$ state only about 2.5 K higher energy. This means that the energy difference between the species with different nuclear spin weights is much smaller than the corresponding difference for H_2O or H_2CO. The torsional $\tau = 2, 4$ states are about 16 K above the $\tau = 1, 3$ states. This difference stems from the tunneling through the *trans* barrier and is comparable to the gas kinetic

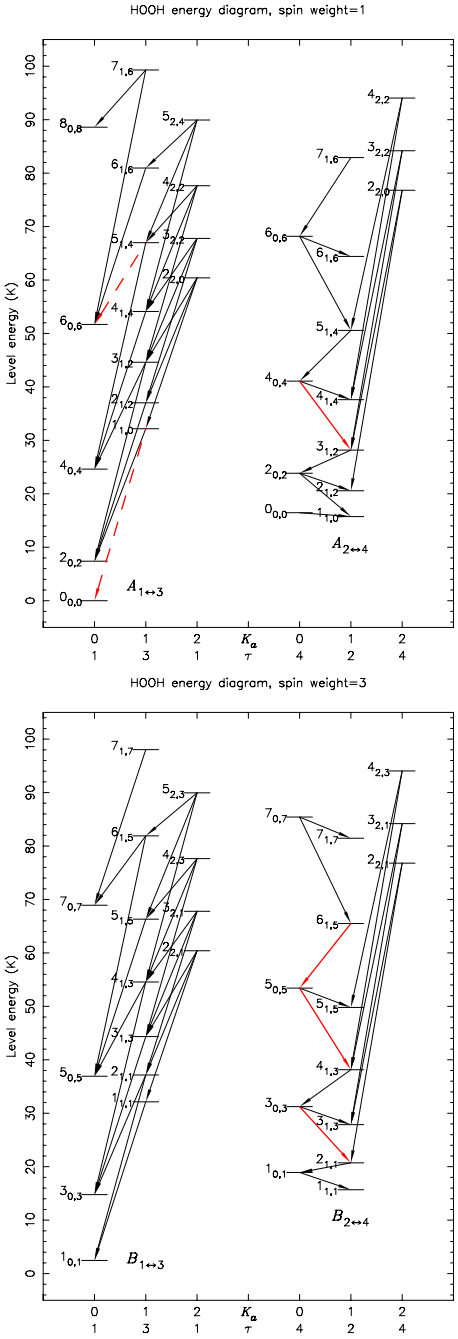

Fig. 1. HOOH energy level diagrams. The energy is given in K on the vertical axis, and at the bottom the quantum numbers K_a and τ are shown. To the left of each level the rotational quantum numbers J_{K_a,K_c} are listed. The *upper* diagram shows the levels with a nuclear spin weight of 1 ($A_{1\leftrightarrow3}$ and $A_{2\leftrightarrow4}$), while those levels with a spin weight of 3 ($B_{1\leftrightarrow3}$ and $B_{2\leftrightarrow4}$) are shown in the *lower* diagram. The allowed c-type transitions within each of the four ladders are indicated as arrows. The red arrows represent detected lines, while the red-dashed arrows indicate non-detections.

temperatures of 20–30 K found in ρ Oph A (Loren et al. 1990; Liseau et al. 2003; Bergman et al. 2011).

In Fig. 2 we show the HOOH spectra toward the core of ρ Oph A. The upper five spectra are toward the SM1 core, α(J2000) = $16^h26^m27.2^s$ and δ(J2000) = −24°24′04″. The 670 GHz CHAMP$^+$ spectrum is an average of all pixels and is centered 30″ north of the SM1 position (usually denoted SM1N). In Fig. 3 spectra of the 219 166 MHz line for the

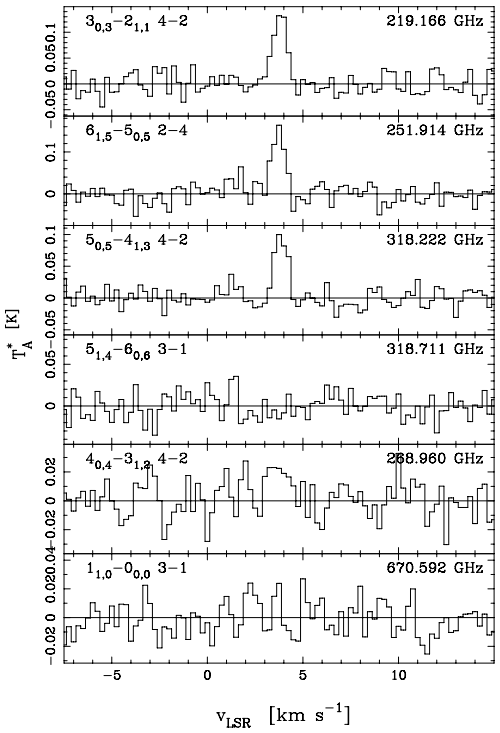

Fig. 2. HOOH spectra toward ρ Oph A. The transition is indicated in each spectrum. The T_A^* intensity scale is in K and the velocity (v_{LSR}) scale is in km s^{-1}. The velocity resolution is 0.25 km s^{-1}.

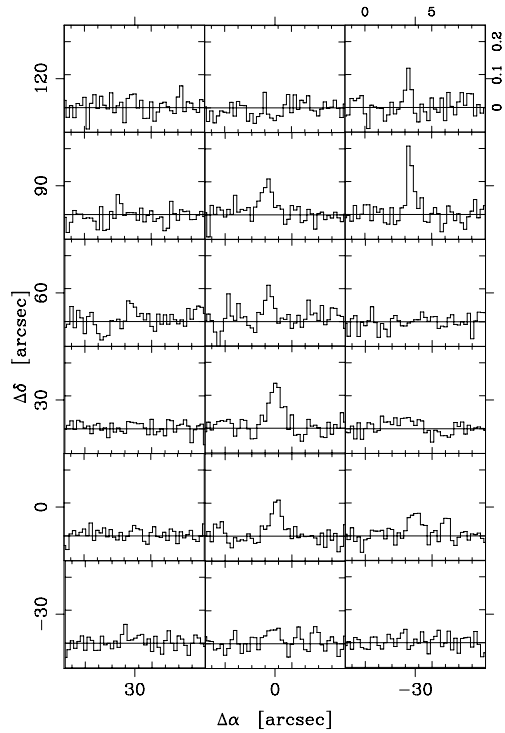

Fig. 3. Map spectra of the 219 166 MHz HOOH line toward ρ Oph A. The map offset (0″, 0″) corresponds to the SM1 position. The T_A^* intensity scale, in K, and the velocity (v_{LSR}) scale, in km s^{-1}, are indicated in the upper right spectrum. The velocity resolution is 0.25 km s^{-1}.

Table 2. Observed HOOH line velocities, widths, and intensities.

Freq. (MHz)	Beam size (arcsec)	v_{LSR} (km s^{-1})	$FWHM$ (km s^{-1})	$\int T_{mb}\,dv^a$ (K km s^{-1})
219 167	28	3.8	0.84	0.167(0.018)
251 915	25	3.7	0.75	0.165(0.018)
268 961	23	3.7	(1.2)	0.040(0.011)
318 223	20	3.8	0.78	0.106(0.013)
318 712	20			<0.044
670 596	9			<0.12^b
				<0.051^c

Notes. $^{(a)}$ Integr. from 2.5 to 4.5 km s^{-1}, errors are 1σ, upper limits are 3σ; $^{(b)}$ average value from three pixels closest to the SM1 position; $^{(c)}$ average value from all pixels, central pixel on SM1N.

observed map positions are shown. In the southern part the line is centered at 3.7 km s^{-1}, while further north, at offset (0″, +60″), the line is at 3.2 km s^{-1}. This NS velocity gradient is almost identical to the one seen for H_2CO and its deuterated variants (Bergman et al. 2011). The narrow peaks to the NW are adjacent to where the sulphur species peak as noted by the same authors. In addition to the map in Fig. 3, we also mapped the 251 GHz line, albeit with a poorer S/N ratio and will not discuss it further here.

The beam sizes, velocity-integrated main-beam brightness temperatures ($\int T_{mb}\,dv$) , fitted LSR velocities (v_{LSR}), and line widths ($FWHM$) are tabulated in Table 2. The T_{mb}-scale was established assuming main-beam efficiencies of 0.75, 0.73, and 0.4, for APEX-1, 2, and CHAMP$^+$, respectively. The upper limits are 3σ and for the CHAMP$^+$ line two intensities are listed in Table 2; one for the three pixels closest to the SM1 position and the other by averaging data from all pixels. The tabulated errors and upper limits depend only on the channel noise.

Using the integrated line intensities in Table 2 (corrected by a beam-filling factor corresponding to a source size of 24″, see Bergman et al. 2011), we performed a rotation diagram analysis (Goldsmith & Langer 1999). From this we can determine the rotation temperature, T_{rot}, as well as the HOOH column density, N(HOOH). The resulting rotation diagram is displayed in Fig. 4. The fit is based on the detected $\tau = 2 \leftrightarrow 4$ lines. We derive $T_{rot} = 22 \pm 3$ K and a total HOOH column density of $(8 \pm 3) \times 10^{12}$ cm^{-2} where the errors depend on the uncertainty of the integrated intensities and a calibration uncertainty of 10–15%. This rotation temperature is very close to the estimates of the kinetic temperatures from H_2CO at the SM1 position. Obviously, the non-detection of the $\tau = 1 \leftrightarrow 3$ lines (open squares in Fig. 4) is not consistent with the fit. Especially the 670 GHz line should have been detected given these values of T_{rot} and N(HOOH). Hence, we conclude that the $\tau = 1, 3$ states are not populated according to a simple LTE model. The non-detection of the 670 GHz line could be a result of subthermal excitation. The spontaneous rate coefficient is large (Table 1) and for a typical value of a collision coefficient ($\sim 10^{-10}$ cm^3 s^{-1}), the critical density of the 670 GHz transition is about two orders of magnitude higher than the H_2 density determined from H_2CO and CH_3OH observations in the same source (Bergman et al. 2011). From the energy diagrams (Fig. 1) it is clear that there is a lack of radiative de-excitation routes out of the $K_a = 0$ levels in the $\tau = 1, 3$ states (as opposed to the $\tau = 2, 4$ states). The population of the $\tau = 1, 3$ states could therefore be confined to the $K_a = 0$ levels if the collisional excitation is inefficient. However, a full statistical equilibrium analysis is needed for understanding the details of the excitation. This also requires some basic knowledge of the collision coefficients. For now we assume that the $\tau = 1, 3$ population is negligible compared to the $\tau = 2, 4$

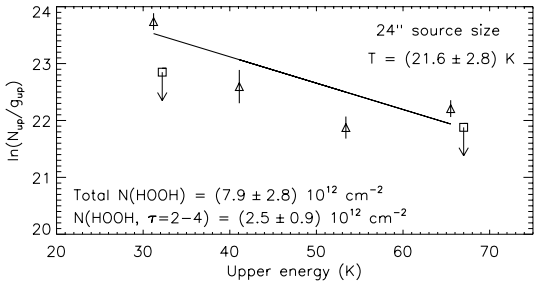

Fig. 4. HOOH rotation diagram. The detected lines (only $\tau = 2 \leftrightarrow 4$ lines) are shown as open triangles with error bars. The size of the error bars corresponds to the total uncertainty (noise and calibration). The 3σ upper limits (not included in the fit) are shown as open squares and downward arrows and originate from transitions between $\tau = 1, 3$ states. The fitted rotation temperature is noted, as is the total column density. The column density for unpopulated $\tau = 1, 3$ states is also given.

population. In this case, we instead find a total molecular column density of $(3 \pm 1) \times 10^{12}$ cm^{-2}.

3. Discussion

Given the good agreement of the velocities of our detected HOOH lines (together with the ≈0.1 km s^{-1} accuracy of the laboratory frequencies) with those from other species we are very confident that the lines belong to HOOH. From our mapping of the 219 GHz line it is also evident that the NS velocity gradient seen for HOOH reflects that of other species. Moreover, the derived rotation temperature of 22 ± 3 K is what would be expected for the ρ Oph A cloud core. For this fairly low excitation temperature one would not expect many lines from other species to be present and, using the JPL and Cologne databases (Pickett et al. 1998; Müller et al. 2005), we found no lines from other species that could possibly interfere with the identification. Of course, the narrow lines (with $FWHM$ typically <1 km s^{-1}) seen toward the ρ Oph A cloud core also make line confusion much less likely.

From the H_2CO and CH_3OH analysis of the SM1 core Bergman et al. (2011) determined an H_2 column density of 3×10^{22} cm^{-2}. Assuming that the HOOH level populations mainly reside in the $\tau = 2, 4$ states, we arrive at an HOOH abundance of about 1×10^{-10}. This is well below the limit of 4.5×10^{-10} found toward Orion KL by Blake et al. (1987).

According to current gas-phase schemes (e.g., the OSU chemical reaction database), formation of HOOH in the gas phase is not efficient. Only two very slow reactions are proposed for its formation, reaction of H_2 with HO_2, or reaction of two OH radicals.

On grains, HOOH is formed through successive hydrogen additions to O_2. This was first proposed by Tielens & Hagen (1982), based on theoretical arguments. Recent laboratory experiments have been made to investigate this route, up to formation of water molecules:

$$O_2 + H + H \rightarrow HOOH \quad (1)$$

$$HOOH + H \rightarrow H_2O + OH. \quad (2)$$

Miyauchi et al. (2008) have investigated the reaction of H atoms with solid O_2 at 10 K. Subsequently, Ioppolo et al. (2008) have investigated the same reaction in the temperature range 12–28 K. Both studies showed that the conversion of O_2 stops at some point before exhaustion of O_2 because of shielding of O_2 in the deepest layers. The experiment of Ioppolo et al. (2008) shows that the shielding decreases with increasing temperature, pointing to the fact that the O_2 ice may become more porous when close to its sublimation temperature (30 K).

Because this shielding may not be very relevant in space, Oba et al. (2009) investigated the formation of HOOH and H_2O when codeposing O_2 and H in the temperature range 10–40 K. The H_2O/HOOH ratio in the formed ices is observed to depend strongly on the temperature, and on the O_2/H flux. The measured H_2O/HOOH ratio is lower than 5 in all experiments (T = 10, 20 K and O_2/H-flux between 3.8×10^{-4} and 1.9×10^{-2}), although higher values may be obtained in the case of lower O_2/H-flux. The present detection of HOOH may open the possibility to quantify the importance of reactions (1) and (2) in the formation of water.

Ioppolo et al. (2008) have modeled the formation of water in typical dense clouds (their Fig. 4). The laboratory results lead to a revision of the energy barriers involved in the models, and their new model (only accounting for the three main routes of water formation on the grains) predicts a fractional abundance for HOOH of a few 10^{-14} with respect to H nuclei. This is more than three orders of magnitude lower than our detection.

Further understanding will require detailed chemical modeling of grain chemistry. This will be the scope of a forthcoming paper. The observation of water in the ρ Oph A region with the *Herschel* Observatory as well as the confirmation of the O_2 detection would also be very valuable in setting constraints on the models.

Acknowledgements. We acknowledge the excellent observational support from the APEX staff. We are grateful to A. Gusdorf for doing some of the CHAMP$^+$ observations. B.P. is funded by the Deutsche Forschungsgemeinschaft (DFG) under the Emmy Noether project number PA1692/1-1.

References

André, P., Ward-Thompson, D., & Barsony, M. 1993, ApJ, 406, 122
Bergman, P., Parise, B., Liseau, R., & Larsson, B. 2011, A&A, 527, A39
Blake, G. A., Sutton, E. C., Masson, C. R., & Phillips, T. G. 1987, ApJ, 315, 621
Boudin, N., Schutte, W. A., & Greenberg, J. M. 1998, A&A, 331, 749
Clancy, R. T., Sandor, B. J., & Moriarty-Schieven, G. H. 2004, Icarus, 168, 116
Cohen, E. A., & Pickett, H. M. 1981, J. Mol. Spectr., 87, 582
Encrenaz, T., Bézard, B., Greathouse, T. K., et al. 2004, Icarus, 170, 424
Goldsmith, P. F., & Langer, W. D. 1999, ApJ, 517, 209
Güsten, R., Nyman, L. Å., Schilke, P., et al. 2006, A&A, 454, L13
Hartogh, P., Jarchow, C., Lellouch, E., et al. 2010, A&A, 521, L49
Helminger, P., Bowman, W. C., & de Lucia, F. C. 1981, J. Mol. Spect., 85, 120
Hougen, J. T. 1984, Can. J. Phys., 62, 1392
Hunt, R. H., Leacock, R. A., Wilbur Peters, C., & Hecht, K. T. 1965, J. Chem. Phys., 42, 1931
Ioppolo, S., Cuppen, H. M., Romanzin, C., van Dishoeck, E. F., & Linnartz, H. 2008, ApJ, 686, 1474
Kasemann, C., Güsten, R., Heyminck, S., et al. 2006, in SPIE Conf. Ser., 6275
Larsson, B., Liseau, R., Pagani, L., et al. 2007, A&A, 466, 999
Liseau, R., Larsson, B., Brandeker, A., et al. 2003, A&A, 402, L73
Liseau, R., Larsson, B., Bergman, P., et al. 2010, A&A, 510, A98
Loren, R. B., Wootten, A., & Wilking, B. A. 1990, ApJ, 365, 269
Miyauchi, N., Hidaka, H., Chigai, T., et al. 2008, Chem. Phys. Lett., 456, 27
Motte, F., André, P., & Neri, R. 1998, A&A, 336, 150
Müller, H. S. P., Schlöder, F., Stutzki, J., & Winnewisser, G. 2005, J. Mol. Struc., 742, 215
Oba, Y., Miyauchi, N., Hidaka, H., et al. 2009, ApJ, 701, 464
Pelz, G., Yamada, K. M. T., & Winnewisser, G. 1993, J. Mol. Spect., 159, 507
Perrin, A., Flaud, J.-M., Camy-Peyret, C., et al. 1996, J. Mol. Spect., 176, 287
Petkie, D. T., Goyette, T. M. J. H. J., De Lucia, F. C., & Helminger, P. 1995, J. Mol. Spect., 171, 145
Pickett, H. M., Poynter, R. L., Cohen, E. A., et al. 1998, J. Quant. Spec. Radiat. Transf., 60, 883
Tielens, A. G. G. M., & Hagen, W. 1982, A&A, 114, 245
Vassilev, V., Meledin, D., Lapkin, I., et al. 2008, A&A, 490, 1157